remote sensing

MDPI

Article

An Investigation of Impacts of Surface Waves-Induced Mixing on the Upper Ocean under Typhoon Megi (2010)

Wenqing Zhang [1,2,*], Rui Li [1,2], Donglin Zhu [3], Dongliang Zhao [1,2] and Changlong Guan [1,2]

[1] Frontier Science Center for Deep Ocean Multispheres and Earth System (FDOMES) and Physical Oceanography Laboratory, Ocean University of China, 238 Songling Road, Qingdao 266100, China
[2] College of Oceanic and Atmospheric Sciences, Ocean University of China, 238 Songling Road, Qingdao 266100, China
[3] Guangxi Key Laboratory of Marine Environmental Science, Guangxi Beibu Gulf Marine Research Center, Guangxi Academy of Sciences, Nanning 530007, China
* Correspondence: wqzhang@ouc.edu.cn

Abstract: Surface waves play an essential role in regulating the mixing processes in the upper ocean boundary, and then directly affect the air–sea exchange of mass and energy, which is important for the intensity prediction of tropical cyclones (TCs). The relative and integrated impacts of the wave breaking (WB) and the wave orbital motion (WOM) on the mixing and ocean response to TC forcing are investigated under typhoon Megi (2010), using the modeled data from a fully coupled air–sea–wave model. It is shown that the WOM can effectively increase the turbulence mixing in the upper ocean, thus significantly deepening the mixing layer depth and cooling the sea surface temperature. The WB can modulate the mixing layer depth and sea surface temperature to some extent in the cold tail zone with a shallow mixing layer (owing to typhoon forcing), whereas the WOM plays a predominant role. On the aspect of ocean currents driven by typhoon winds, the WOM-induced mixing significantly weakens the current velocity and shear strength in the upper ocean mixing layer, while the relative contribution for turbulence production between the WOM and the current shear differs at different vertical regions. Moreover, the effect of the WOM on the upper ocean turbulent mixing are dependent on the location with respect to the typhoon center, the local vertical thermal structure, and surface wave states.

Keywords: mixing; typhoon; wave orbital motion; wave breaking

Citation: Zhang, W.; Li, R.; Zhu, D.; Zhao, D.; Guan, C. An Investigation of Impacts of Surface Waves-Induced Mixing on the Upper Ocean under Typhoon Megi (2010). *Remote Sens.* **2023**, *15*, 1862. https://doi.org/10.3390/rs15071862

Academic Editor: Yukiharu Hisaki

Received: 5 March 2023
Revised: 27 March 2023
Accepted: 29 March 2023
Published: 30 March 2023

1. Introduction

The upper ocean boundary or mixed layer plays a critical role in regulating the earth environment, which involves all aspects of oceanic and atmospheric change. For example, the development of a tropical cyclone (TC) and its intensity are sensitively dependent on the thermal structure and sea surface temperature (SST) of the upper mixed layer [1,2], as TCs are intense air–sea interaction phenomena and gain energy such as the latent and sensible heat from the upper ocean to intensify. For another example, in the process of air–sea gas exchange, such as carbon dioxide, methane, and nitrous oxide (important greenhouse gases after water vapor), their exchange rates are affected by the turbulence in the surface ocean where wave breaking can greatly enhance the turbulence [3,4]. In terms of air–sea fluxes of mass and energy, the physical process of turbulent mixing in the upper ocean plays an import role in controlling weather and climate change [4]. However, there are still some gaps in current knowledge about the mixing process of the upper ocean [4].

The underestimation for the mixed layer depth (MLD) and the overestimation for the SST usually occur in the existing oceanic models when simulating the upper ocean in summer [5,6]. It is believed that some physical processes (such as surface waves) related

to the upper ocean turbulence mixing are absent in oceanic models, leading to insufficient mixing.

Surface waves are considered to play an important role in regulating the upper ocean turbulent mixing. Some field observations and simulations have indicated that wave breaking (WB) increases mixing near the ocean surface, but has a minor or non-significant effect on SST and MLD, although the observed characteristics of dissipation rate under the condition of WB can be well-simulated [7–9].

Recently, the mixing owing to wave orbital motion (WOM) has received extensive concern. Offshore observations [10] and laboratory experiments [11–13] have shown that WOM generates turbulence and enhances mixing [14]. Unlike WB, which influences the turbulence and mixing to the depth at the wave height scale, WOM injects turbulence deeply at the scale of wave length, which is much larger than wave height [14]. In numerical studies, it is suggested that the overestimated SST and underestimated MLD are significantly improved if including the mixing owing to WOM into global oceanic or climate models [15–17].

Langmuir turbulence, the phenomena of interaction between Stokes drifts and small-scaled vorticities generated by surface winds and waves, is another wave-related mechanism for enhancing the turbulence mixing in the upper ocean [18–20]. Some simulation results show that ocean models represent the upper ocean thermal structure well when Langmuir turbulence is explicitly resolved [21,22]. However, parameterization of Langmuir turbulence for ocean models remains a challenge. There are great differences between current Langmuir turbulence schemes, which obscure the Langmuir effect magnitude under realistic forcing [23].

Under some extreme conditions, particularly TC conditions, complicated changes occur for the ocean currents and surface waves due to the frequently changing and rotating winds. Thus, the turbulence generation and mixing of the upper ocean are complex problems and have not been resolved completely. The influence of WOM on the ocean turbulent mixing under the condition of a TC were reported in a few studies [24,25], but the integrated effect of WOM and WB has not been discussed. Although the WB is considered to play a limited role in deepening the MLD, it can also have an effect on the SST change and turbulent dissipation, especially under a shallow mixed layer [8,9,26], which is very important for the air–sea interface gases exchange [3]. Moreover, concurrently resolving both WOM and WB in the coupled air–sea–wave model makes the model involved with complete physical processes and in accord with the real situation. In this paper, the Langmuir turbulence effect is not discussed to avoid potential overmixing. It is still not completely clear whether the mixing processes due to the WOM and Langmuir circulation have an overlap [27]. Moreover, it is quite difficult to distinguish between WOM-induced mixing and Langmuir turbulence, as they coexist and both are related to water particle orbits.

During October in 2010, the typhoon center of Megi moved across the middle of two moorings deployed in the South China Sea (SCS). These two moorings were very close to the typhoon track, and measured rare profiles for current and temperature under the typhoon condition, which provided us a precious chance to study the upper ocean mixing and response under the condition of a TC. In this study, we analyzed and discussed the influence of WOM and WB on the mixing and response of upper ocean under typhoon Megi (2010), adopting observed data from the two moorings and simulated results from a coupled air–sea–wave model [28]. The rest of this paper is organized as below: introductions of typhoon Megi (2010), mooring observations, model information related to the simulated results, and the mixing parameterizations of WOM and WB are described in Section 2; observed and modeled results and analysis are shown in Section 3; the mixing induced by surface waves in different regions and stages under typhoon Megi (2010) is discussed in Section 4; the conclusions and summaries are listed in Section 5.

2. Data and Methods

Our previous paper [28] discussed the effect of mixing owing to WOM and WB on the intensity and size for typhoon Megi (2010), using a fully coupled air–sea–wave model system. In this paper, we use our previous model results [29] which were validated using various observations to focus on the effect of waves-induced mixing on the response of upper ocean to TC forcing. Here, we just describe the key information about the coupled model, the domain and period for the simulation, and numerical experiments. We do not repeat the model parameter and scheme settings for brevity. For more information on the model parameter and scheme settings, please read the paper by Zhang et al. [28] for reference.

2.1. Typhoon Megi (2010) and Observations

Typhoon Megi began to develop as a tropical depression on 13 October 2010 in the western North Pacific, then headed to the west and moved across the Philippines on 18 October. When it entered SCS on 19 October, it quickly made a sharp turn and moved northward. On 23 October, Megi made its final landfall on the south coast of China. Before Megi's first landfall in the Philippines, the maximum wind speeds near Megi center reached about 70 m/s which is the maximum intensity during Megi. While passing through the Philippines, Megi's intensity was significantly decreased, then increased rapidly again after it entered SCS. After 6:00 UTC on 20 October, Megi began to decay slowly.

There were two moorings which were quite close to Megi center at 00:00 UTC on 22 October; the right mooring (RM) was at 21°03.59′N, 118°25.61′E, about 25 km to the right of Megi's center; the left mooring (LM) was at 21°06.57′N, 117°52.66′E, about 30 km to the left of Megi's center (Figure 1). RM and LM, equipped with Acoustic Doppler Current Profilers, measured the ocean currents from about 400 m to 40 m with 8m vertical resolution and 180 s temporal interval [30]. RM, equipped with 28 thermometers and 2 CTDs, measured the ocean temperature from about 360 m to 60 m with 10 m vertical resolution and 60 s temporal interval [30]. The raw measurements were preprocessed by linear interpolation in the vertical direction and averaging every 30 min, providing data with temporal and vertical resolution of 30 min and 5 m.

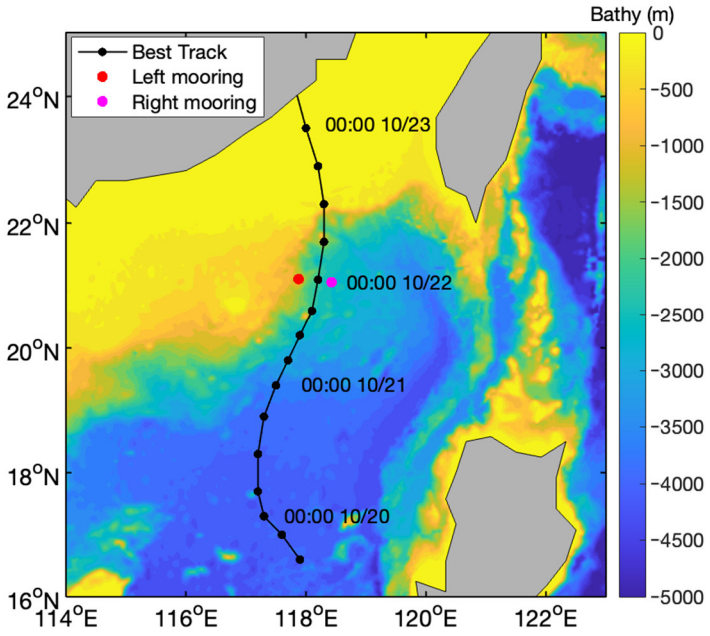

Figure 1. Best track (black line with dot) for typhoon Megi (2010) moving in the SCS, locations of two mooring buoys, and topography of the SCS. The magenta and red dots display the positions for the right and left mooring buoys, respectively.

In the work by Zhang et al. [28], these simulated results of typhoon track, intensity, size, sea surface temperature, sea subsurface temperature, surface winds, and surface waves for Megi were validated using best track data developed by Joint Typhoon Warning Center (JTWC), observations provided by Remote Sensing System (RSS), the RM described above, and altimeters of JASON-1 and -2. In this paper, we did not repeat the validation for these simulated results for brevity; however, we used the observed currents from the two mooring buoys to verify the modeled currents.

2.2. Description for the Coupled Model and Simulation

Here, we simply describe the coupled ocean–atmosphere–wave–sediment transport (COAWST) (v3.1) model [2]. This model was used for the simulation in Zhang et al. [28] and produced the simulated data for our investigation. COAWST (v3.1) includes three main components: the Advanced Research Weather Research and Forecasting (WRF) model; the Regional Ocean Modeling System (ROMS); and the Simulating Waves Nearshore (SWAN) mode.

WRF contains various schemes and parameterizations for physical processes, which is widely applicable to predictions of atmospheric motions at different scales and research experiments [31]. SWAN involves a variety of wave-related actions, such as refraction, wave–wave interactions, wave dissipation, and shoaling [32]. ROMS is usually utilized to simulate the ocean environment, such as ocean temperature, currents, etc., by solving the Reynolds-Averaged Navier–Stokes (RANS) equations with a terrain-following coordinate. In the coupling between WRF and ROMS, SSTs are sent from ROMS to WRF, and momentum and heat fluxes are transferred back to ROMS (Figure 2). In the coupling between SWAN and WRF, wave parameters, i.e., wave period, wave length, and significant wave height, are sent from SWAN to WRF, and 10 m winds are passed back to SWAN. In the coupling between ROMS and SWAN, ocean surface elevation, current, and bathymetry from ROMS are sent to SWAN, and wave parameters calculated by SWAN, such as percent wave breaking, wave length, significant wave height, etc., are exchanged back to ROMS. For more complete and detailed information about this model, please refer to Warner et al. [2].

The simulation domain covered the northern SCS. WRF, ROMS, and SWAN have the same horizontal grid points of 220 × 256 with 6 km spatial resolution. The simulation period was from 12:00 UTC on 19 October to 00:00 UTC on 23 October. For more details about the model settings, initial and boundary conditions, please refer to Zhang et al. [28].

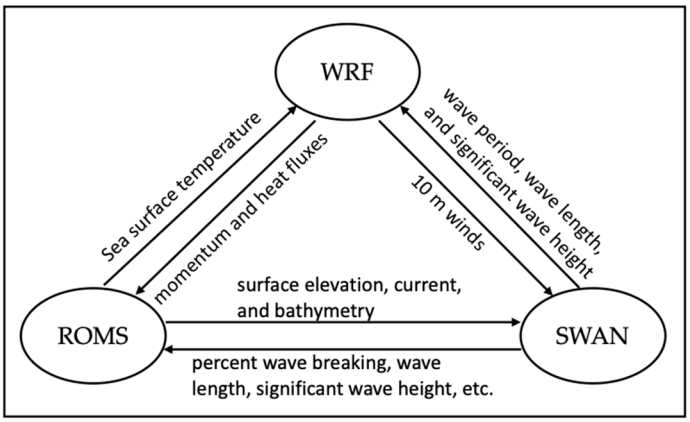

Figure 2. Data exchange between three components, i.e., WRF, ROMS, and SWAN, in COAWST.

2.3. Parametrization Scheme of Wave-Induced Mixing

2.3.1. Wave Orbital Motion

The turbulent source item induced by WOM, abbreviated as P_W, was added by Zhang et al. [28] into a generic length scale (GLS) turbulence closure scheme [33,34] incorporated in COAWST:

$$\frac{D}{Dt}(k) = \frac{\partial}{\partial z}\left[\frac{\nu_t}{\sigma_k}\frac{\partial}{\partial z}(k)\right] + P_s + P_w + P_b - \varepsilon \quad (1)$$

and

$$\frac{D\psi}{Dt} = \frac{\partial}{\partial z}\left(\frac{\nu_t}{\sigma_\psi}\frac{\partial \psi}{\partial z}\right) + \frac{\psi}{k}(c_1(P_s + P_w) + c_3 P_b - c_2 \varepsilon F_{wall}) \quad (2)$$

where k represents the turbulent kinetic energy (TKE); P_b and P_s are the turbulent productions owing to buoyancy and current shear, respectively; ε represents the TKE dissipation rate; F_{wall} is a wall function; ψ is a generic parameter; c_1, c_2, c_3 are constant coefficients; σ_ψ and σ_k represent Schmidt numbers of ψ and k, respectively; and ν_t is the eddy viscosity. P_W is calculated by the following equation [35]:

$$P_W = b_1 k_w \omega_p^3 \frac{{H_s}^3}{8} e^{3k_w z} \quad (3)$$

where b_1 is a dimensionless coefficient, setting as the constant of 0.0014 following previous studies [24,28,36]; H_s, ω_p, and k_w are significant wave height, peak wave radian frequency, and wave number, respectively. z represents the water depth with negative values in ocean.

2.3.2. Wave Breaking

The mixing induced by WB is considered as a turbulence source for ocean surface. COAWST provides an option to incorporate the effect of WB on mixing, adopting the parameterization proposed by Craig and Banner [8]. In COAWST, WB is introduced into the GLS turbulence closure scheme (i.e., Equations (1) and (2)) through boundary conditions [37]:

$$\frac{\nu_t}{\sigma_k}\frac{\partial}{\partial z}(k) = \overline{\varepsilon_w},\ z{=}\zeta \quad (4)$$

$$\begin{aligned}\frac{\nu_t}{\sigma_\psi}\frac{\partial \psi}{\partial z} &= -\frac{\sigma_k}{\sigma_\psi}\cdot\left(c_\mu^0\right)^p \cdot i \cdot k^{i-1}\cdot\left(\kappa\cdot(z_0 - z)\right)^j \cdot y \\ &-\frac{\nu_t}{\sigma_\psi}\cdot\left(c_\mu^0\right)^p \cdot j \cdot k^i \cdot \kappa \cdot \left(\kappa\cdot(z_0 - z)\right)^{j-1},\ z{=}\zeta\end{aligned} \quad (5)$$

where κ is the von Karman constant; $\overline{\varepsilon_w}$ is the TKE flux due to WB; c_μ^0, i, j, and p are constant coefficients; z_0 represents the surface roughness; y is set to $\overline{\varepsilon_w}$ on the surface.

2.4. Numerical Experiments

We chose four experiments which were conducted in the simulations of Zhang et al. [28] to investigate the influence of mixing due to WB and WOM on the upper ocean for Megi. Table 1 summarizes these four experiments.

Table 1. Experiments for typhoon Megi to evaluate the relative and integrated impacts of turbulent mixing due to wave breaking (WB) and wave orbital motion (WOM).

Expts.	Description
E0	Exclude WB and WOM
E1	Include WB
E2	Include WOM
E3	Include both WB and WOM

3. Results

We presented and compared the model results of SST, MLD, current, etc., among different experiments to study the relative and integrated effects of WOM and WB on the upper ocean under typhoon forcing, and did not validate the simulated typhoon track, intensity, subsurface temperature, SST, surface wind speed, and surface waves using observed data as the verification for these modeled results was performed by Zhang et al. [28].

3.1. SST and MLD

The validations for SST and MLD (the depth with a bias of 0.5 °C for ocean temperature compared with the SST) in Zhang et al. [28] indicated that the simulated MLDs, SSTs, and subsurface temperature matched the measurements from RM and RSS well, especially in E2 and E3. Comparing the modeled SSTs and MLDs in experiments (E1, E2, and E3) including wave-induced mixing with the control experiment E0, it was generally shown that the WB resulted in a tiny decrease for SST and a slight increase for MLD, whereas the WOM led to a great SST decrease and a large MLD increase (Figures 3 and 4).

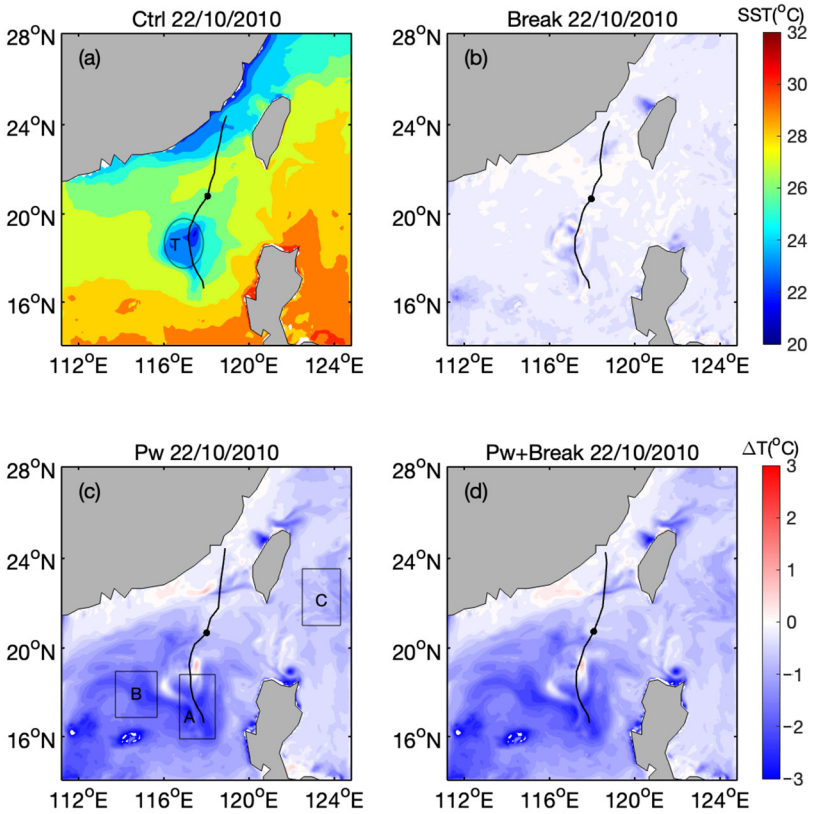

Figure 3. Simulated daily mean SST in different numerical experiments on 22 October 2010. (**a**) SST in the control experiment excluding wave-induced mixing. (**b**–**d**) Deviations of SST compared with the control experiment for each of the three experiments including mixing owing to surface waves (i.e., considering only the mixing owing to wave breaking, only the mixing owing to wave orbital motion, and both these two factors). The black dot indicates the position of Megi's center at 00:00 UTC on 22 October 2010. The black line represents Megi's track. The ellipse marked with "T" in the panel (**a**) represents the classic cold tail zone behind Megi's center. Text boxes marked with "A", "B", and "C" in the panel (**c**) display three different and representative analysis areas.

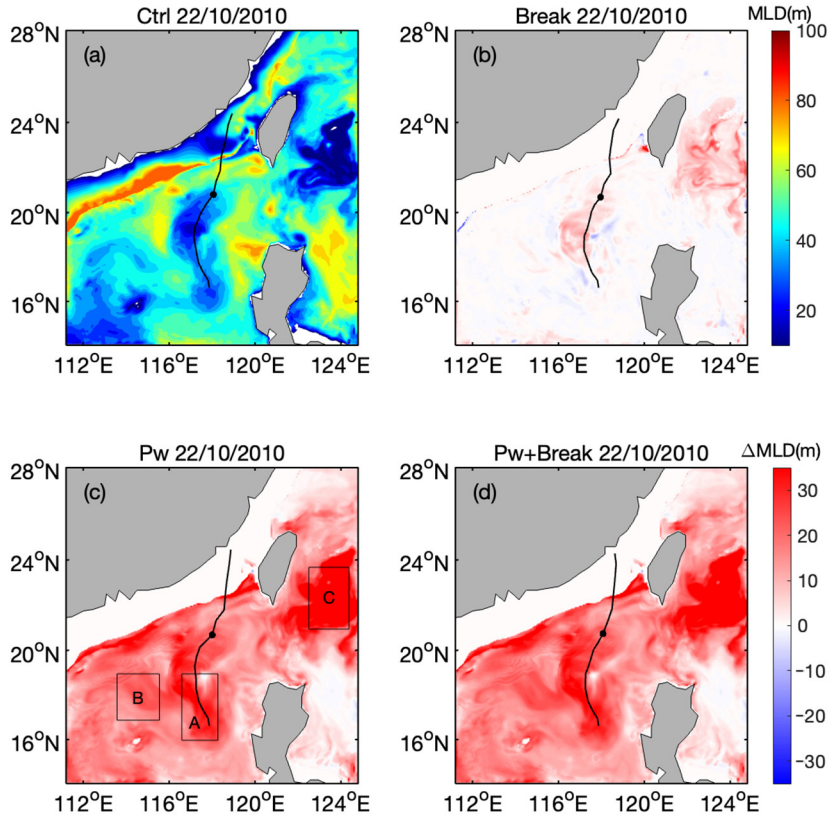

Figure 4. Same as Figure 3, but for MLD. (**a**) MLD in the control experiment excluding wave-induced mixing. (**b**–**d**) Deviations of MLD compared with the control experiment for each of the three experiments including mixing owing to surface waves.

In the classic cold tail zone (shown in Figure 3a and marked with "T") along Megi's track and behind Megi's center, where the MLD was shallow (about 20 m), the WB cooled the SST by about 0.5 °C and deepened the MLD by 5–10 m, whereas it did not effectively cool the SST or deepen the MLD in the other zone with relative deep MLD (Figures 3b and 4b). The simulated results in E2 showed that the mixing induced by WOM cooled SST and deepened MLD much greater than the WB (Figures 3c and 4c), and suggested a trend in the region along Megi's track that the shallower the mixing layer, the more the mixing layer (SST) was deepened (decreased). Note that the effect of the mixing induced by WOM on MLD and SST was dependent on the local vertical thermal structure and surface wave states. We chose two typical and different areas to study the effects of WOB on the MLD and SST at different spatial regions which were forced by typhoon winds, but had different responses to typhoon forcing. For example, in the zone along typhoon track (zone A shown in Figures 3c and 4c), a large amount of cold water was pumped up due to Ekman pumping, then the thermocline was uplifted and the MLD became shallow with the value of ~25 m in E0 (Figure 4a). The WOM can penetrate turbulence into a deep depth at wave length scale which may reach approximately 100 m under typhoon conditions, significantly enhancing the upper ocean mixing, so the MLD in zone A was deepened obviously (increased by 20–30 m), and the SST is decreased markedly (reduced by about 2.0 °C), compared with E0. In the zone without Ekman pumping (zone B shown in Figures 3c and 4c), the surface waves were still large due to the typhoon forcing, so the WOM injected the turbulence deeply enough and entrained colder water from below the mixed layer base or thermocline, leading to obvious MLD deepening and SST cooling. The MLD (SST) in E2 was 25 m deeper (2.0 °C cooler) than in E0 in zone B. In the zone far away from the typhoon, such as zone C shown in the Figures 3c and 4c, there was an obvious deepening

for MLD in E2, but the SST cooling seemed relatively small. This was an interesting and seemingly unusual result. The main reason for this scenario was the local seasonal thermocline and relatively small surface waves. As shown in Figure 5, in zone C, there was a very shallow MLD (~10 m) and a weak seasonal thermocline near the surface, and below the seasonal thermocline was a profound mixing layer, and the bottom of this main mixing layer was as deep as about 70 m. When the mixing induced by WOM was taken into account (in E2), the seasonal thermocline disappeared due to the enhanced mixing induced by WOM. However, the local WOM did not influence deeply the lower part or the bottom of the main mixing layer which is below the initial seasonal thermocline, as the surface waves were relatively small at this location (see Figure 11 in Zhang et al. [28]). As shown in Figure 6, the turbulence production induced by WOM *Pw* in zone C was quite small, about two orders of magnitude smaller than in zones A and B (note the different color bars in different panels), and the depth of the isoline for 1×10^{-5} m^2/s^3 in the zone C was about 30 m, much shallower than the bottom of the main mixing layer, indicating that the mixing owing to WOM in the zone C influenced to the relative shallow depth. Although the modeled MLDs in E2 showed that the MLD in the zone C was deepened significantly (more than 50 m compared with E0), the value of MLD in the zone C actually represented the depth of main mixing layer base. Additionally, the difference for the water temperature between the main mixing layer and the ocean surface was small, so the reduction of SST in E2 was small. It was also noticed that in the zone C, the MLD was obviously deepened by ~10 m after considering WB in E1. This was also due to the local shallow MLD above the seasonal thermocline as described above. In this area, the local wave height was about 6~7 m (see Figure 11 in Zhang et al. [28]), and the WB effectively changed the local shallow MLD.

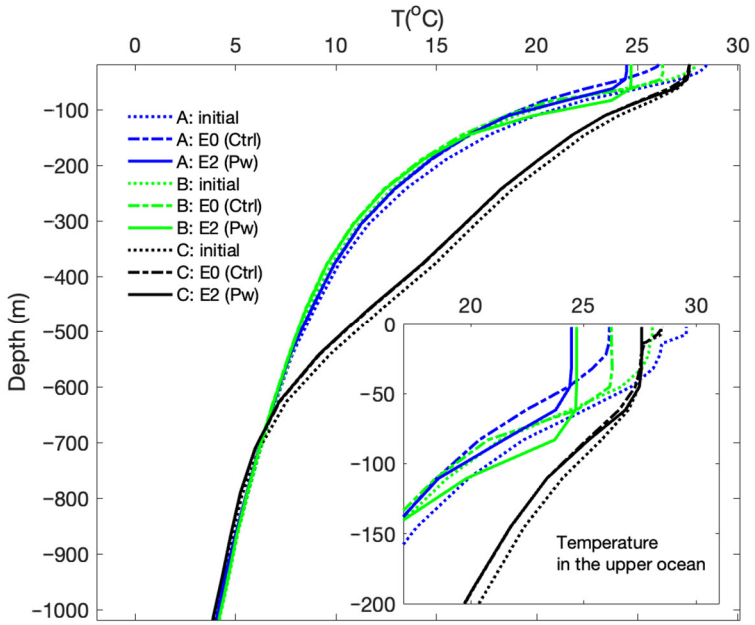

Figure 5. Water temperature profiles in zones A, B, and C at the initial time (dotted lines) and on 22 October (dash-dotted and solid lines).

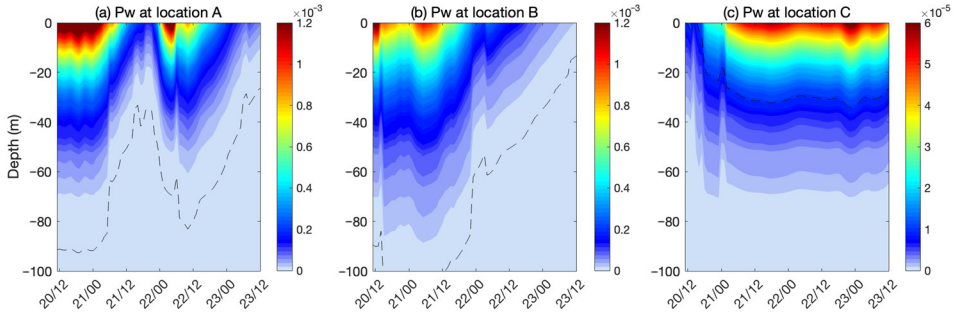

Figure 6. The turbulence production induced by wave orbital motion P_W (m^2/s^3) at locations A, B, and C in experiment E2. The black dashed lines represent the isoline of 1×10^{-5} m^2/s^3.

In E3, both WOM and WB were considered, and the modeled results for SST and MLD were almost the same as those in E2, indicating that the WOM had an overpowering influence on the upper ocean turbulence mixing compared with WB, whereas the effect of mixing owing to WB was negligible compared with WOM-induced mixing [28].

3.2. Sea Surface and Subsurface Currents

In this subsection, the influence of surface waves-induced mixing on the ocean currents driven by typhoon winds was analyzed. The observed currents obtained from two moorings (LM and RM) were utilized to verify the simulated results. Note that the observation data of ocean currents from 60 m to the ocean surface was absent. In order to study the impacts of mixing owing to WB and WOM on ocean current field under typhoon winds more clearly, the tides were removed from the observed and simulated currents. Firstly, both the movements at high frequency and errors in measurement were removed from the observed currents using a low-pass filter following Zou et al. [30]. Then, the tide currents which were calculated by the tidal analysis program T_TIDE [38] were removed. Figure 7 presents the tide currents and the currents after removing tides at the LM and the RM.

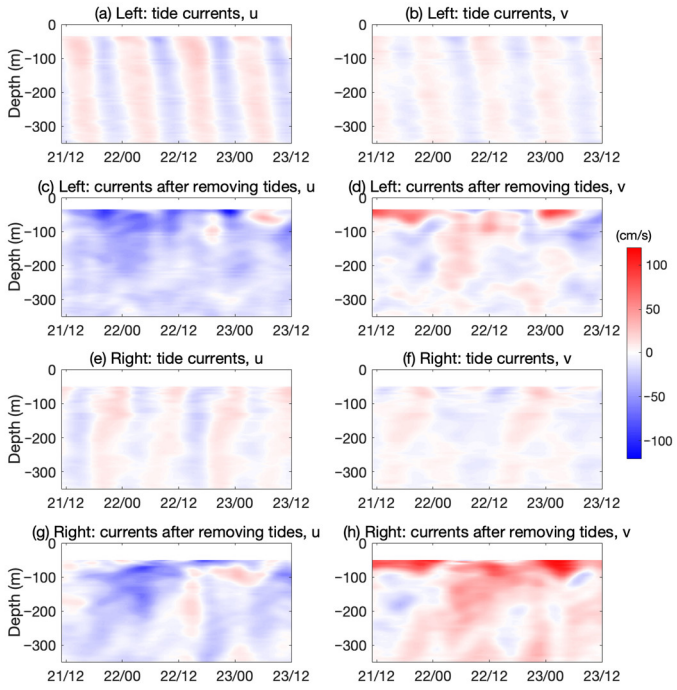

Figure 7. The tide currents and the currents after removing tides at the left and right mooring buoys. Left and right panels display the eastward component (u) and the northward component (v) of current velocity, respectively.

Figures 8 and 9 are the modeled currents (tides removed) of four experiments at the locations of LM and RM, respectively. Generally, the simulated currents (below 60 m) agreed with the observations reasonably. The biases between the modeled results and the observed currents may be attributed to the model grid resolution, the error of typhoon track, and the method used to process the observed data from moorings. Some common scenarios were observed and captured in the mooring observations and modeled results: (1) The currents driven by typhoon winds in the upper layer were more powerful on the right of Megi's center than on the left. This difference was owing to the same directions between wind stress and near-inertial current on the right of Megi's track, whereas opposite directions on the left [39]. (2) Near-inertial oscillations (NIOs) were active at almost all depths, and stronger in the mixed layer, and became more evident after the passage of Megi. Guan et al. [40] found that NIOs decayed rapidly within two inertial periods (33.3 h at RM and 33.4 h at LM) after Megi passed. Note that our simulation period did not cover this quick damping of NIOs.

Comparing the simulated subsurface currents among the different experiments (Figures 8 and 9), it was found that the surface waves-induced mixing weakened the current velocity and shear strength in the upper mixed layer. In E1 considering only WB, the modeled results were slightly weaker than those in E0, indicating that the WB had a small effect on the ocean currents, as it did for SST and MLD. In E2, including the WOM-induced mixing, the simulated currents were significantly weakened by 40% in the upper mixed layer, compared with E0. The modeled sea surface currents of E1 and E2 were also weaker with varying degrees than in E0 (Figure 10) in areas affected by typhoon forcing, similarly to the scenarios of subsurface currents. In E3 with both WB and WOM, the modeled results for the surface and subsurface currents were almost the same as those in E2, indicating that the WOM overpowered the WB with absolute predominance in terms of ocean currents driven by typhoon winds.

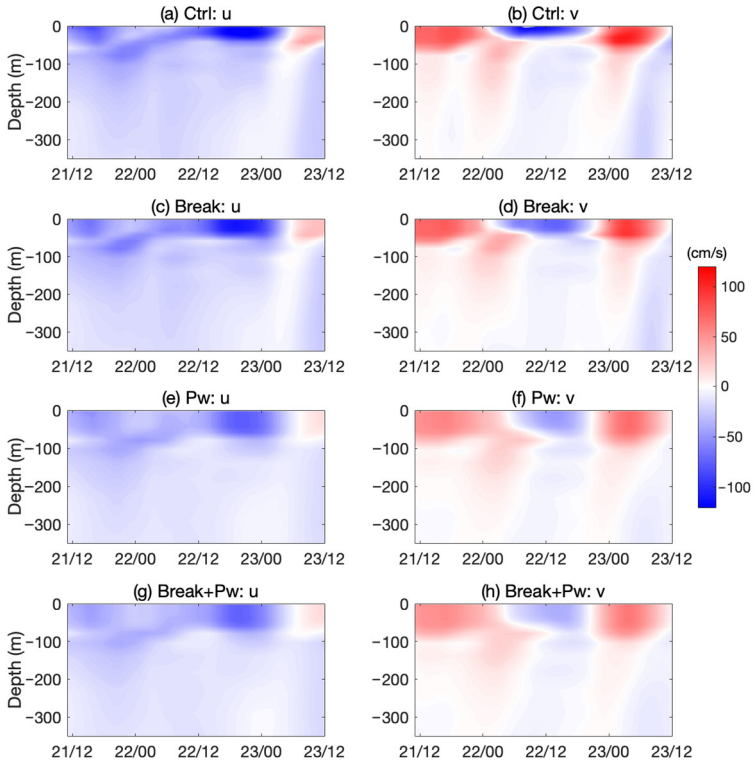

Figure 8. The modeled currents (removed tides) of four experiments at the location of the left mooring. Left and right panels display the eastward component (u) and the northward component (v) of current velocity, respectively.

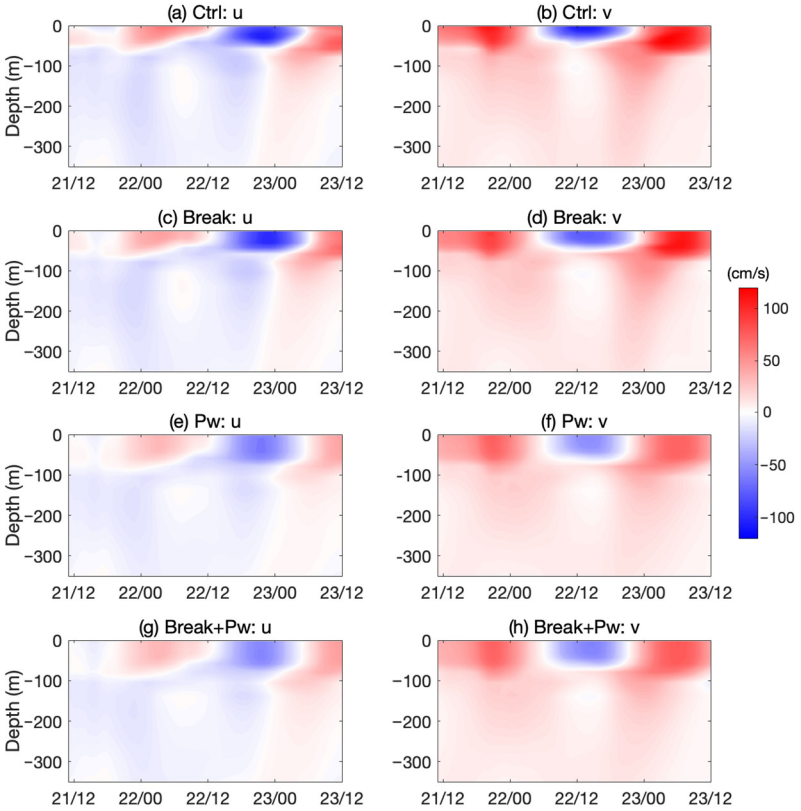

Figure 9. Same as Figure 8, but at the location of the right mooring.

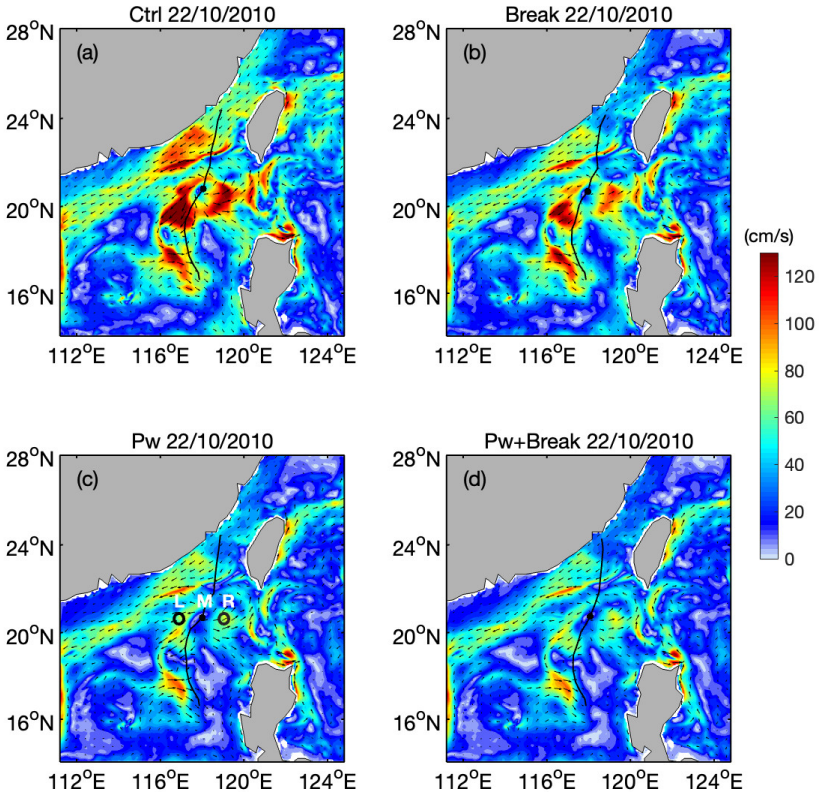

Figure 10. Sea surface currents (removed tides) simulated in different experiments at 00:00 UTC on 22 October 2010. The black dot in the panel (**c**) represents the typhoon center (M) at 00:00 UTC on 22 October. Two black circles in the panel (**c**) represent the locations of the right (R) and left (L) sides of Megi's center (M).

4. Discussion

In this section, we discussed the mixing and turbulence production owing to surface waves in the upper ocean under typhoon forcing. Figure 11 displays the TKE among different experiments at locations of the typhoon center (M), the right (R), and the left (L) sides of Megi's center (indicated in Figure 10c). In E1 with WB, the TKE was strongly increased, about two orders of magnitude larger than that in E0, and the maximum TKE appeared at the ocean surface. In E2 with WOM, the TKE was about one order of magnitude larger than that in E0. The greatest value of TKE was at some depth below the sea surface and the TKE near the surface was quite small, which was what we would expect as the vortex's size should be restricted near the surface [35]. Although the maximum value of TKE induced by WB in E1 was much larger than that induced by WOM in E2, the influencing depth of WB was shallower than WOM. The effect of WB was limited to the very shallow depth, and did not effectively impact the mixing at deeper depth. As shown in Figure 11, the depth of TKE isoline of 1×10^{-3} m^2/s^2 in E1 was quite similar to that in E0, whereas the depth of TKE isoline of 1×10^{-3} m^2/s^2 in E2 was much deeper to that in E0, indicating the WOM injected turbulence deeply. In addition, when both these two wave-related mixing processes were considered in E3, the maximum TKE appeared under the sea surface and was consistent with the value in E1, much larger than in E2, implying that the WOM may also penetrate turbulence induced by WB to deeper depth. Note that the depth of TKE isoline of 1×10^{-3} m^2/s^2 in E3 is almost the same as in E2, suggesting that the mixing due to WOM was predominant compared with WB.

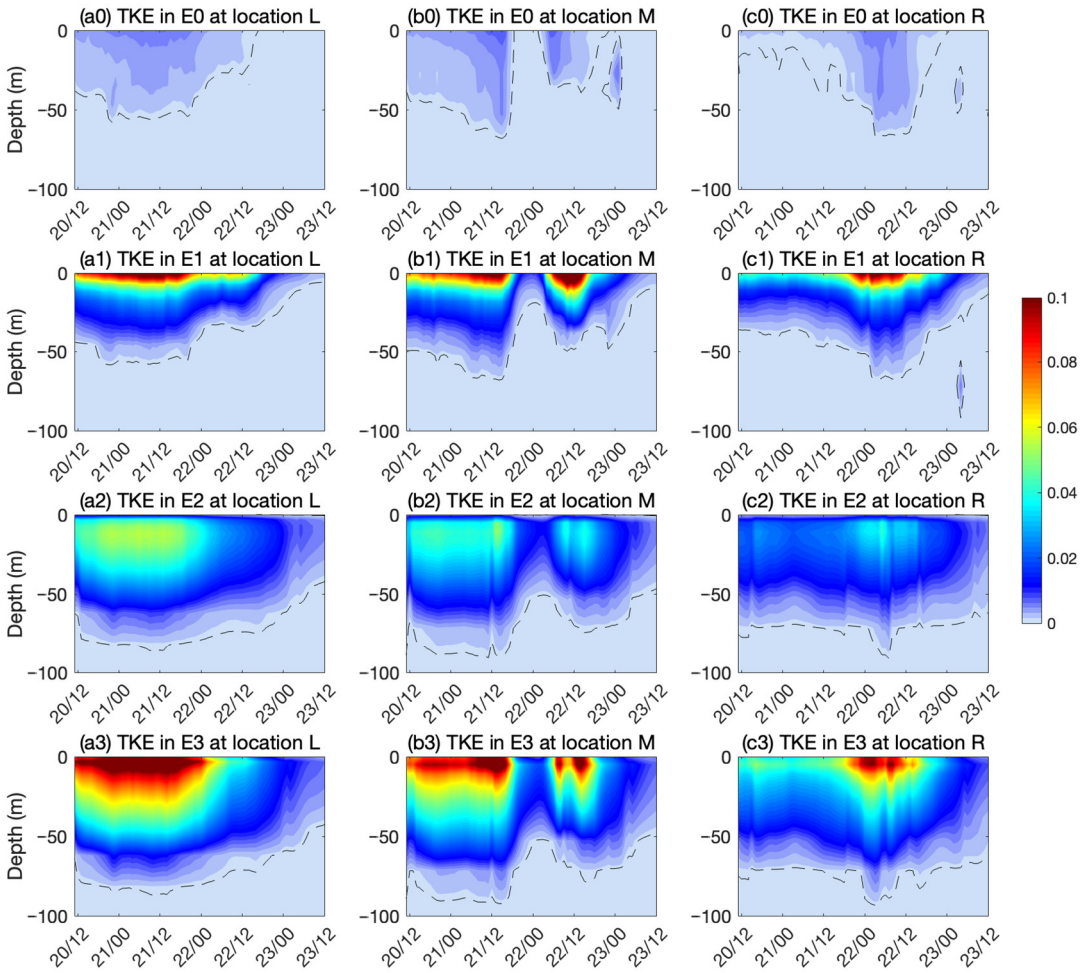

Figure 11. TKE (m^2/s^2) among different experiments at locations of L, M, and R (indicated in Figure 10c). The black dashed lines represent the isoline of 1×10^{-3} m^2/s^2.

Complex and frequently changing currents and waves occur under typhoon forcing. The current shear and wave-induced turbulence are the main sources of turbulence production. The relative importance between the current shear and WOM differs at different regions. As shown in Figure 12a–c, the WOM had a predominant impact in the upper region of the mixing layer with $Pw/Ps > 1$, whereas the current shear was comparable to or little greater than the WOM near the bottom of the mixing layer. This variation was owing to the attenuation of WOM from the ocean surface (as shown in Figure 6) and the enhancement of current shear at the bottom of the mixing layer (as displayed in Figures 8 and 9).

During Megi, the current shear and WOM-induced turbulence productions changed quickly. For example, before Megi's center reached the location M, the *Pw* was about two orders of magnitude greater than *Ps*, resulting in deepening the mixed layer (Figure 12b). When the typhoon center approached near location M (about six hours before 00:00 UTC on 22 October), the ratio of *Pw*/*Ps* enhanced rapidly, and the *Pw* was about four orders of magnitude greater than *Ps* in the upper region of the mixing layer. The underlying cause for this scenario was that the ocean currents in the typhoon eye were rather weak, while the surface waves were relatively strong with the significant heights of about 8 m (see Figure 11 in Zhang et al. [28]). Thus, the *Pw* was absolutely predominant compared with *Ps* in this situation. After the typhoon center passed through the location M, the scenario of cold suction due to Ekman pumping began (Figure 12e), the ratio of *Pw*/*Ps* decreased, and the *Pw* was about two orders of magnitude greater than *Ps*. Then, when the typhoon center moved far away from the location M (about 20 h later), the ratio of *Pw*/*Ps* re-increased, and *Pw* was about three orders of magnitude larger than *Ps*. Although the typhoon center was far away from the location M, there was still large surface waves in the local area, dominating TKE production and mixing in the upper ocean, finally deepening MLD. In the left and right sides of Megi's center forced by high typhoon winds, i.e., the locations of L and R, it was shown that WOM-induced TKE production always overpowered the TKE production from current shear, especially after the typhoon center moved far away (Figure 12a,c), as it did at the location of M.

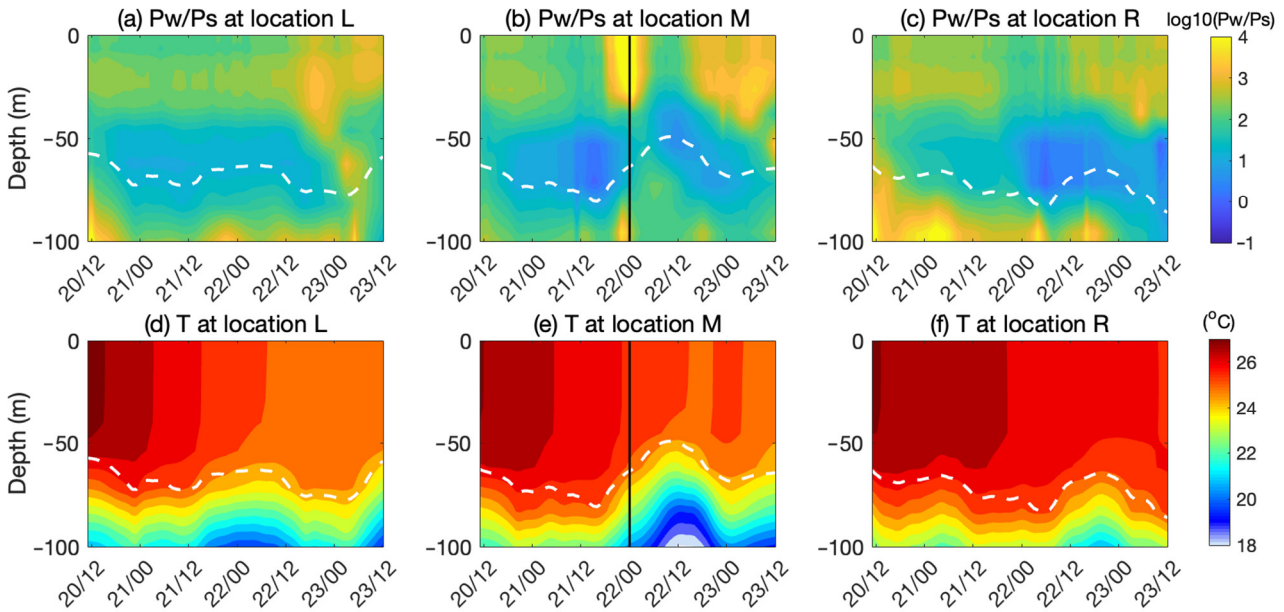

Figure 12. (**a**–**c**) The ratio of the shear production (*Ps*) and wave orbital motion-induced turbulence production (*Pw*) in different zones of L, M, and R of experiment E2. (**d**–**f**) The temperature in different zones of L, M, and R of experiment E2. The black vertical lines in panels (**b** and **e**) display the time when typhoon center passed. The MLDs are marked by white dashed lines.

In the aspect of the TKE dissipation rate ε, WB and WOM-induced mixing can obviously enhance the ε, and WOB has a more significant impact than WB. As shown in Figure 13, when the wave-induced mixing was not taken into account (E0), the area with high value of ε was mainly concentrated in the region very close to the surface. When the WB-induced mixing was considered in E1, the ε in the upper ocean boundary was increased significantly compared with E0, whereas the region with effective values of the ε (larger than the background ε with the value of 1×10^{-8}~1×10^{-7} m^2/s^3) was not deepened. For example, the depth of isolines of 1×10^{-7} m^2/s^3 in E1 was basically the same as in E0. This is consistent with our understanding that the effect of WB on deepening the mixed layer is quite limited. In E2, which included the WOB-induced mixing, the distribution of the ε was significantly different from that in E1 and E0. The area with effective values of the ε in E2 was obviously deepened, i.e., the isoline of 1×10^{-7} m^2/s^3 was deepened by about 80~100 m compared with E0 or E1. When the WB and WOM were considered together in E3, the characteristics of ε in most regions were almost consistent with E2. These results implied that WOM played a dominant role in regulating the ε in the upper ocean boundary compared with WB. The current results of ε were from numerical simulation, which need to be verified by more observations under TC conditions in the future.

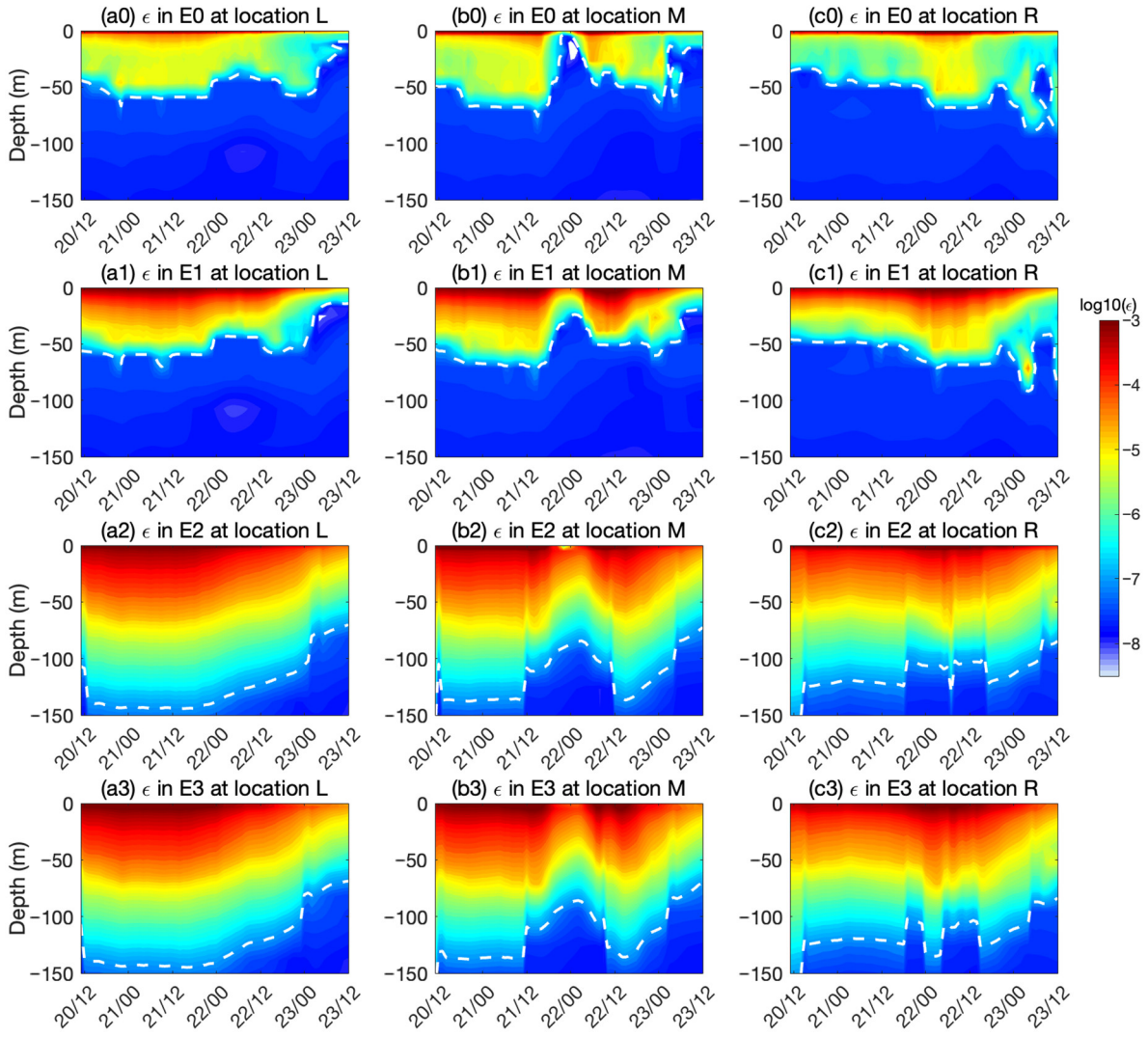

Figure 13. TKE dissipation rate ε (m^2/s^3) among different experiments at locations of L, M, and R (indicated in Figure 10c). The white dashed lines represent the isoline of 1×10^{-7} m^2/s^3.

5. Conclusions

The relative and integrated impacts of mixing owing to WOM and WB on the response of upper ocean to typhoon Megi (2010) in SCS were investigated, adopting the simulated results from Zhang et al. [28] and observations from two mooring buoys near to the typhoon track.

Comparing simulated results among different experiments showed that the WOM significantly enhanced the mixing of the upper ocean, resulting in extensive MLD deepening and great SST cooling, which is consistent with previous studies [24,25]. Under typhoon Megi (2010) conditions, the wave breaking had a non-negligible effect on regulating MLD and SST at locations with a shallow MLD (at wave height scale), e.g., cold tail zone, while the WOM played a dominant role. When considering the WOM and WB concurrently, the WOM may also penetrate turbulence induced by wave breaking near the surface to some deep depth, but much shallower than the influence depth of WOM. Note that the impact of wave orbital motion on MLD and SST was dependent on the local vertical thermal structure and surface wave states. In the zone with a local seasonal thermocline and relatively small surface waves, the mixing induced by WOM can make the seasonal thermocline disappear, but its influencing depth is shallow. Thus, the MLD displayed as the depth of the main mixing layer bottom, and a slight SST cooling, was exhibited.

On the aspect of currents in the upper ocean driven by typhoon winds, it was found that wave-induced mixing weakened current velocity and shear strength of the upper mixing layer. The relative importance of current shear and WOM for turbulence productions differed at different regions. In the upper area of the mixing layer, WOM played a dominant role, i.e., $Pw/Ps > 1$, whereas the current shear was comparable to or little greater than the wave orbital motion at the depth near the base of the mixing layer. Furthermore, ocean current shear and WOM-induced turbulence productions changed quickly in the upper area of the mixing layer at different time stages during Megi.

Our study provides a suggestive insight for impacts of mixing induced by WB and WOM on the upper ocean (including at different spatial regions and at different time stages) under the condition of typhoon Megi (2010) in SCS. However, there are a variety of special geographic locations and complex topography in SCS, and various scales of motion are active, e.g., large-scale circulation, mesoscale eddies, and internal tides. In our present work, we do not consider the interactions between these different scales motions or surface waves-induced mixing. Moreover, only one typhoon case was selected to be studied in this paper, and this typhoon moved slowly in SCS, which provided the upper ocean enough time to respond to the typhoon forcing [41]. Typhoon processes with different characteristics cause different ocean responses. For example, a typhoon with sudden path change can make the oceanic responses much more remarkable than the one moving straight [42]. Furthermore, typhoons moving in different oceanic regions, e.g., continental shelves or the open ocean, have quite different impacts on the upper ocean [43,44]. Therefore, the effects of wave-induced mixing on the upper ocean under TCs with different natures need to be investigated more. In future work, the surface waves-induced mixing under the modulation by the complex background in SCS, and more case studies based on more reliable and complete observations of atmosphere, ocean, and waves, are required.

Author Contributions: Conceptualization, W.Z. and C.G.; methodology, R.L., W.Z. and D.Z. (Donglin Zhu); validation, W.Z. and D.Z. (Donglin Zhu); formal analysis, D.Z. (Dongliang Zhao); investigation, R.L. and W.Z.; resources, D.Z. (Dongliang Zhao) and W.Z.; data curation, W.Z. and D.Z. (Dongliang Zhao); writing—original draft preparation, W.Z.; writing—review and editing, W.Z., R.L. and D.Z. (Dongliang Zhao); supervision, W.Z.; project administration, W.Z.; funding acquisition, W.Z. All authors have read and agreed to the published version of the manuscript.

Funding: This study was funded and supported by National Natural Science Foundation of China (Grant No. U20A2099) and National Key Research and Development Program of China (Grant No.

2022YFC3105002). Besides, Laoshan Laboratory (Grant No. LSKJ202202401) also provided financial support.

Data Availability Statement: Observed and simulated data utilized in this work can be accessed at https://doi.org/10.6084/m9.figshare.17121335.v4 (accessed on 7 June 2022). JTWC best track data were downloaded from https://www.ncei.noaa.gov/products (accessed on 7 June 2022).

Acknowledgments: The authors appreciate researchers for their work on the simulated data, best track data, and schemes utilized in this study. The authors thank scientists for deploying moorings and providing measurements. The authors are deeply grateful to Sun Jian and Liu Qingxiang for their suggestions and support for this work.

Conflicts of Interest: The authors declare no conflict of interest. The funders had no role in the design of the study; in the collection, analyses, or interpretation of data; in the writing of the manuscript; or in the decision to publish the results.

References

1. Liu, B.; Liu, H.; Xie, L.; Guan, C.; Zhao, D. A Coupled Atmosphere-Wave-Ocean Modeling System: Simulation of the Intensity of an Idealized Tropical Cyclone. *Mon. Wea. Rev*. **2011**, *139*, 132–152. https://doi.org/10.1175/2010mwr3396.1.
2. Warner, J.C.; Armstrong, B.; He, R.; Zambon, J.B. Development of a Coupled Ocean-Atmosphere-Wave-Sediment Transport (COAWST) Modeling System. *Ocean Modell.* **2010**, *35*, 230–244. https://doi.org/10.1016/j.ocemod.2010.07.010.
3. Brooks, I.M.; Yelland, M.J.; Upstill-Goddard, R.C.; Nightingale, P.D.; Archer, S.; D'Asaro, E.; Beale, R.; Beatty, C.; Blomquist, B.; Bloom, A.A.; et al. Physical exchanges at the air-sea interface UK-SOLAS field measurements. *Bull. Amer. Meteor. Soc.* **2009**, *90*, 629–644. https://doi.org/10.1175/2008BAMS2578.1.
4. Breviere, E.; The SOLAS Scientific Steering Committee (Eds). *SOLAS 2015–2025: Science Plan and Organisation*; SOLAS International Project Office, GEOMAR Helmholtz Centre for Ocean Research Kiel: Kiel, Germany, 2016; 76 p. Available online: https://dev.solas-int.org/science/science-plan.html (accessed on 3 January 2023).
5. Kantha, L.H.; Clayson, C.A. An improved mixed layer model for geophysical applications. *J. Geophys. Res.* **1994**, *99*, 25235–25266. https://doi.org/10.1029/94jc02257.
6. Martin, P.J. Simulation of the mixed layer at OWS November and Papa with several models. *J. Geophys. Res.* **1985**, *90*, 903–916. https://doi.org/10.1029/JC090iC01p00903.
7. Burchard, H. Simulating the Wave-Enhanced Layer under Breaking Surface Waves with Two-Equation Turbulence Models. *J. Phys. Oceanogr*. **2001**, *31*, 3133–3145. https://doi.org/10.1175/1520-0485(2001)031<3133:STWELU>2.0.CO;2.
8. Craig, P.D.; Banner, M.L. Modeling Wave-Enhanced Turbulence in the Ocean Surface Layer. *J. Phys. Oceanogr*. **1994**, *24*, 2546–2559. https://doi.org/10.1175/1520-0485(1994)024<2546:MWETIT>2.0.CO;2.
9. Huang, C.J.; Qiao, F.; Song, Z.; Ezer, T. Improving simulations of the upper ocean by inclusion of surface waves in the Mellor-Yamada turbulence scheme. *J. Geophys. Res.* **2011**, *116*, C01007. https://doi.org/10.1029/2010jc006320.
10. Cavaleri, L.; Fox-Kemper, B.; Hemer, M. Wind Waves in the Coupled Climate System. *Bull. Amer. Meteor. Soc*. **2012**, *93*, 1651–1661. https://doi.org/10.1175/bams-d-11-00170.1.
11. Babanin, A.V.; Haus, B.K. On the existence of water turbulence induced by nonbreaking surface waves. *J. Phys. Oceanogr*. **2009**, *39*, 2675–2679.
12. Cheung, T.K.; Street, R.L. The turbulent layer in the water at an air-water interface. *J. Fluid Mech.* **1988**, *194*, 133–151.
13. Dai, D.; Qiao, F.; Sulisz, W.; Han, L.; Babanin, A.V. An experiment on the nonbreaking surface-wave-induced vertical mixing. *J. Phys. Oceanogr.* **2010**, *40*, 2180–2188.
14. Babanin, A.V. On a wave-induced turbulence and a wave-mixed upper ocean layer. *Geophys. Rea. Lett*. **2006**, *33*. https://doi.org/10.1029/2006gl027308.
15. Babanin, A.V.; Ganopolski, A.; Phillips, W.R.C. Wave-induced upper-ocean mixing in a climate model of intermediate complexity. *Ocean Modell*. **2009**, *29*, 189–197. https://doi.org/10.1016/j.ocemod.2009.04.003.
16. Qiao, F.; Yuan, Y.; Yang, Y.; Zheng, Q.; Xia, C.; Ma, J. Wave-induced mixing in the upper ocean: Distribution and application to a global ocean circulation model. *Geophys. Rea. Lett*. **2004**, *31*, L11303. https://doi.org/10.1029/2004gl019824.
17. Song, Y.; Qiao, F.; Song, Z. Improved simulation of the South Asian summer monsoon in a coupled GCM with a more realistic ocean mixed layer. *J. Atmos. Sci.* **2012**, *69*, 1681–1690.
18. Li, M.; Zahariev, K.; Garrett, C. Role of Langmuir circulation in the deepening of the ocean surface mixed layer. *Science* **1995**, *270*, 1955–1957. https://doi.org/10.1126/science.270.5244.1955.
19. McWillams, J.C.; Sullivan, P.P.; Moeng, C.-H. Langmuir turbulence in the ocean. *J. Fluid Mech*. **1997**, *334*, 1–30. https://doi.org/ https://doi.org/10.1017/S0022112096004375.
20. Hughes, C.J.; Liu, G.; Perrie, W.; Sheng, J. Impact of Langmuir turbulence, wave breaking, and Stokes drift on upper ocean dynamics under hurricane conditions. *J. Geophys. Res.- Oceans.* **2021**, *126*, e2021JC017388. https://doi. org/10.1029/2021JC017388.
21. Reichl, B.G.; Wang, D.; Hara, T.; Ginis, I.; Kukulka, T. Langmuir Turbulence Parameterization in Tropical Cyclone Conditions. *J. Phys. Oceanogr*. **2016**, *46*, 863–886. https://doi.org/10.1175/jpo-d-15-0106.1.

22. Zhang, X.; Chu, P.C.; Li, W.; Liu, C.; Zhang, L.; Shao, C.; Zhang, X.; Chao, G.; Zhaop, Y. Impact of Langmuir Turbulence on the Thermal Response of the Ocean Surface Mixed Layer to Supertyphoon Haitang (2005). *J. Phys. Oceanogr*. **2018**, *48*, 1651–1674. https://doi.org/10.1175/jpo-d-17-0132.1.
23. Li, Q.; Reichl, B.G.; Fox-Kemper, B.; Adcroft, A.J.; Belcher, S.E.; Danabasoglu, G.; Grant, A.L.; Griffies, S.M.; Hallberg, R.; Hara, T.; et al. Comparing Ocean Surface Boundary Vertical Mixing Schemes Including Langmuir Turbulence. *J. Adv. Model. Earth Sy.* **2019**, *11*, 3545–3592. https://doi.org/10.1029/2019MS001810.
24. Aijaz, S.; Ghantous, M.; Babanin, A.V.; Ginis, I.; Thomas, B.; Wake, G. Nonbreaking wave-induced mixing in upper ocean during tropical cyclones using coupled hurricane-ocean-wave modeling. *J. Geophys. Res.- Oceans*. **2017**, *122*, 3939–3963. https://doi.org/10.1002/2016jc012219.
25. Toffoli, A.; McConochie, J.; Ghantous, M.; Loffredo, L.; Babanin, A.V. The effect of wave-induced turbulence on the ocean mixed layer during tropical cyclones: Field observations on the Australian North-West Shelf. *J. Geophys. Res.- Oceans*. **2012**, *117*, C00J24. https://doi.org/10.1029/2011jc007780.
26. Sun, Q.; Song, J.; Guan, C. Simulation of the ocean surface mixed layer under the wave breaking. *Acta Oceanol. Sin.* **2005**, *24*, 9–15.
27. Ghantous, M.; Babanin, A.V. Ocean mixing by wave orbital motion. *Acta Phys. Slovaca* **2014**, *64*, 1–57.
28. Zhang, W.; Zhao, D.; Zhu, D.; Li, J.; Guan, C.; Sun, J. A Numerical Investigation of the Effect of Wave-Induced Mixing on Tropical Cyclones Using a Coupled Ocean-Atmosphere-Wave Model. *J. Geophys. Res.- Atmospheres*. **2022**, *127*, e2021JD036290. https://doi.org/10.1029/2021jd036290.
29. Zhang, W. A Numerical Investigation of the Effect of Wave-Induced Mixing on Tropical Cyclones Using a Coupled Ocean-Atmosphere-Wave Model [Dataset]. Figshare. **2021**. Available online: https://figshare.com/articles/dataset/Data_that_supports_the_Summary_Results_Tables_and_Figures_/17121335/4 (accessed on 7 June 2022).
30. Zou, Z.; Zhao, D.; Tian, J.; Liu, B.; Huang, J. Drag coefficients derived from ocean current and temperature profiles at high wind speeds. *Tellus A: Dyn. Meteorol. Oceanogr.* **2018**, *70*, 1463805. https://doi.org/10.1080/16000870.2018.1463805.
31. Skamarock, W.C.; Klemp, J.B.; Dudhia, J.; Gill, D.O.; Barker, D.; Duda, M.G.; Huang, X. –Y.; Wang, W.; Powers, J.G. *A Description of the Advanced Research WRF Version 3*; NCAR Tech; Note NCAR/TN-475+STR. **2008**; 113 p. Available online: https://opensky.ucar.edu/islandora/object/technotes%3A500/datastream/PDF/view (accessed on 2 June 2022).
32. Booij, N.R.R.C.; Ris, R.C.; Holthuijsen, L.H. A third-generation wave model for coastal regions: 1. Model description and validation. *J. Geophys. Res.- Oceans*, **1999**, *104*, 7649–7666. https://doi.org/10.1029/98JC02622.
33. Umlauf, L.; Burchard, H. A generic length-scale equation for geophysical. *J. Mar. Res*. **2003**, *61*, 235–265. https://doi.org/10.1357/002224003322005087.
34. Warner, J.C.; Sherwood, C.R.; Arango, H.G.; Signell, R.P. Performance of four turbulence closure models implemented using a generic length scale method. *Ocean Modell.* **2005**, *8*, 81–113. https://doi.org/10.1016/j.ocemod.2003.12.003.
35. Ghantous, M.; Babanin, A.V. One-dimensional modelling of upper ocean mixing by turbulence due to wave orbital motion. *Nonlinear Proc. Geoph*. **2014**, *21*, 325–338. https://doi.org/10.5194/npg-21-325-2014.
36. Young, I.R.; Babanin, A.V.; Zieger, S. The Decay Rate of Ocean Swell Observed by Altimeter. *J. Phys. Oceanogr*. **2013**, *43*, 2322–2333. https://doi.org/10.1175/jpo-d-13-083.1.
37. Kumar, N.; Voulgaris, G.; Warner, J.C.; Olabarrieta, M. Implementation of the vortex force formalism in the coupled ocean-atmosphere wave-sediment transport (COAWST) modeling system for inner shelf and surf zone applications. *Ocean Modell.* **2012**, *47*, 65–95. https://doi.org/10.1016/j.ocemod.2012.01.003.
38. Pawlowicz, R.; Beardsley, B.; Lentz, S. Classical Tidal Harmonic Analysis Including Error Estimates in MATLAB using t_tide. *Comput. Geosci.* **2002**, *28*, 929–937.
39. Price, J.F. Upper ocean response to a hurricane. *J. Phys. Oceanogr*. **1981**, *11*, 153–175.
40. Guan, S.; Zhao, W.; Huthnance, J.; Tian, J.; Wang, J. Observed upper ocean response to typhoon Megi (2010) in the Northern South China Sea. *J. Geophys. Res. Oceans*. **2014**, *119*, 3134–3157, https://doi.org/10.1002/2013JC009661.
41. Lu, Z.; Wang, G.; Shang, X. Inner-Core Sea Surface Cooling Induced by a Tropical Cyclone. *J. Phys. Oceanogr*. **2021**, *51*, 3385–3400. https://doi.org/10.1175/JPO-D-21-0102.1.
42. Zhang, Y.; Liu, Y.; Guan, S.; Wang, Q.; Zhao, W.; Tian, J. Sudden Track Turning of Typhoon Prapiroon (2012) Enhanced the Upper Ocean Response. *Remote Sens.* **2023**, *15*, 302. https://doi.org/10.3390/rs15020302.
43. Dzwonkowski, B.; Fournier, S.; Lockridge, G.; Liu, Z.; Park, K. Hurricane Sally (2020) Shifts the Ocean Thermal Structure across the Inner Core during Rapid Intensification over the Shelf. *J. Phys. Oceanogr*. **2022**, *52*, 2841–2852. https://doi.org/10.1175/JPO-D-22-0025.1.
44. Zhang, H.; Xie, X.; Yang, C.; Qi, Y.; Tian, D.; Xu, J.; Cai, S.; Wu, R.; Ma, Y.; Ni, X.; et al. Observed impact of Typhoon Mangkhut (2018) on a continental slope in the South China Sea. *J. Geophys. Res.- Oceans.* **2022**, *127*, e2022JC018432. https://doi.org/10.1029/2022JC018432.